

## Supporting Information

High Aspect Ratio Cylindrical Microdomains Oriented Vertically on the Substrate using Block Copolymer Micelles and Temperature-Programmed Solvent Vapor Annealing

Sungnam Kim,<sup>a</sup> Gumhye Jeon,<sup>b</sup> Sung Woo Heo,<sup>a</sup> Hye Jeong Kim,<sup>b</sup> Seung Bin Kim,\*<sup>a</sup> Taihyun Chang,\*<sup>a</sup> and Jin Kon Kim\*<sup>b</sup>

<sup>a</sup>*Department of Chemistry,*

*Pohang University of Science and Technology, Pohang, 790-784, Korea,*

<sup>b</sup>*National Creative Research Center for Block Copolymer Self-Assembly and Department of*

*Chemical Engineering,*

*Pohang University of Science and Technology, Pohang, 790-784, Korea*

\* Corresponding authors:

jkkim@postech.edu (jkk), sbkim@postech.edu (sbk), and tc@postech.edu (tc)

## 1. Characterization of PS-*b*-P4VP-C and PS-*b*-P4VP-L in bulk state

Fig. S1 shows SAXS profile ( $I(q)$ ) versus  $q$  ( $= 4\pi \sin\theta / \lambda$ ), in which  $q$  is the scattering vector and  $2\theta$  is the scattering angle) measured at room temperature, and TEM image, respectively, for PS-*b*-P4VP-C in bulk. The sample was placed in an aluminum holder sealed with two pieces of 8  $\mu\text{m}$  Kapton film and annealed at 200 °C for 48 h to obtain the equilibrium morphology, followed by quenching to room temperature. Due to the characteristic peak positions of 1,  $\sqrt{3}$ ,  $\sqrt{7}$ ,  $\sqrt{12}$  relative to the first order peak ( $q^* = 0.102 \text{ nm}^{-1}$ ) in SAXS profile, PS-*b*-P4VP-C has hexagonally packed cylinder microdomains. The diameter ( $D$ ) of P4VP cylinder from SAXS profile is calculated

as 45 nm by using  $D = 2d \sqrt{\left(\frac{2f}{\sqrt{3}\pi}\right)}$  with  $d = 2\pi/q^*$  and  $f_{\text{P4VP}} = 0.36$ .<sup>1</sup> Also, from the TEM image,

hexagonally packed cylindrical microdomains consisting of the P4VP block are clearly seen. The diameter ( $D$ ) of P4VP cylindrical microdomains is 37 nm, which is obtained from the inset of the TEM image. The discrepancy of  $D$  measured by SAXS and TEM can be attributed to the staining contrast or deformation during microtoming.<sup>2</sup>

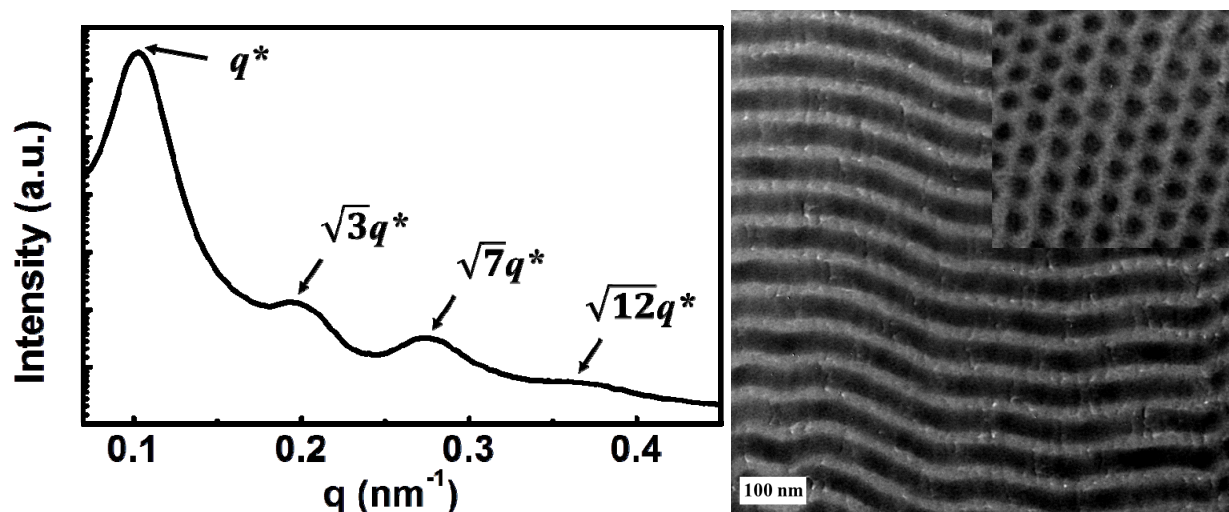


**Fig. S1.** SAXS profile measured at room temperature and TEM image (longitudinal direction view) of PS-*b*-P4VP-C in bulk. The inset of TEM image is the cross-sectional view.

Fig. S2 shows SAXS profile measured at room temperature and TEM image for PS-*b*-P4VP-L in bulk. Due to the characteristic peak positions of 1, 2, 3, 4 relative to the first order peak ( $q^* = 0.150 \text{ nm}^{-1}$ ) in SAXS profiles, PS-*b*-P4VP-L has lamellar microdomains. Also, TEM image clearly demonstrates the lamellar microdomains.

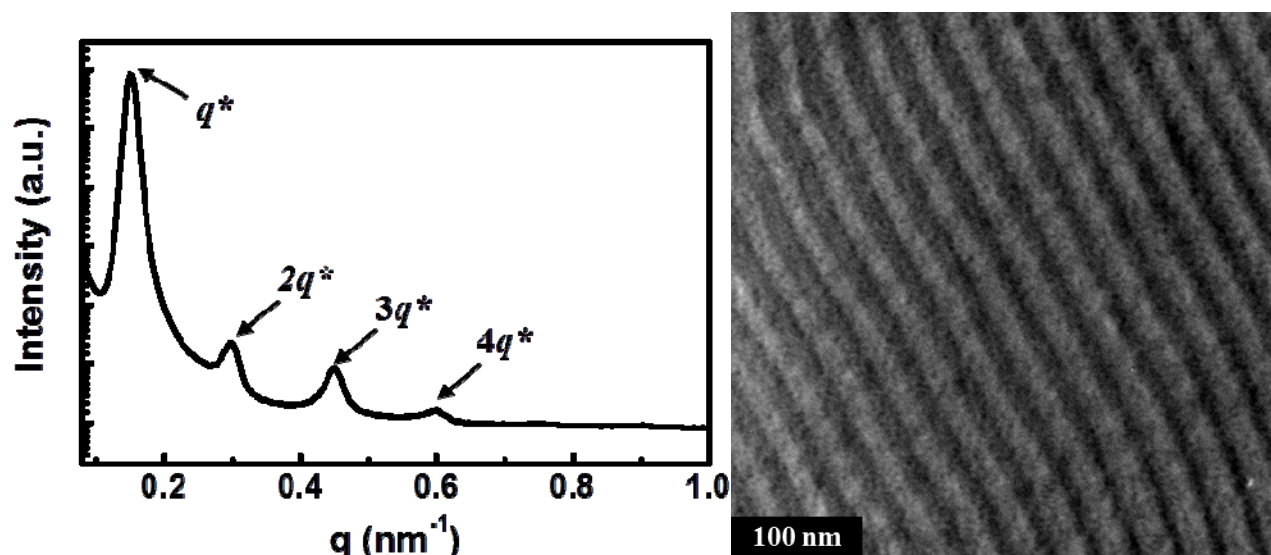


**Fig. S2.** SAXS profiles measured at room temperature and TEM images of PS-*b*-P4VP-L.

## 2. Characaterization of the PS-*b*-P4VP-C thin film at the large area before and after solvent vapor annealing

The grazing incidence-SAXS (GI-SAXS) patterns were obtained to check the arrangement of cylinders in a large area for the solvent vapor-annealed film and the result is shown in Fig. S3. High order scattering peaks at  $\sqrt{3} q^*$  and  $\sqrt{7} q^*$  are only observed along  $q_{xy}$  axis, although the intensity of these two peaks is much smaller than  $q^*$  peak. The existence of higher order peaks is very evident in one-dimensional SAXS profile along  $q_{xy}$  direction, as shown in Fig. S3(b), which is obtained from 2-D GI-SAXS pattern. These scattering peaks satisfied the Bragg conditions for hexagonally packed cylinders oriented normal to the substrate. Since there are no arcs (or ring patterns) related to  $q^*$ , the cylindrical microdomains are oriented vertically on a substrate in a large area.

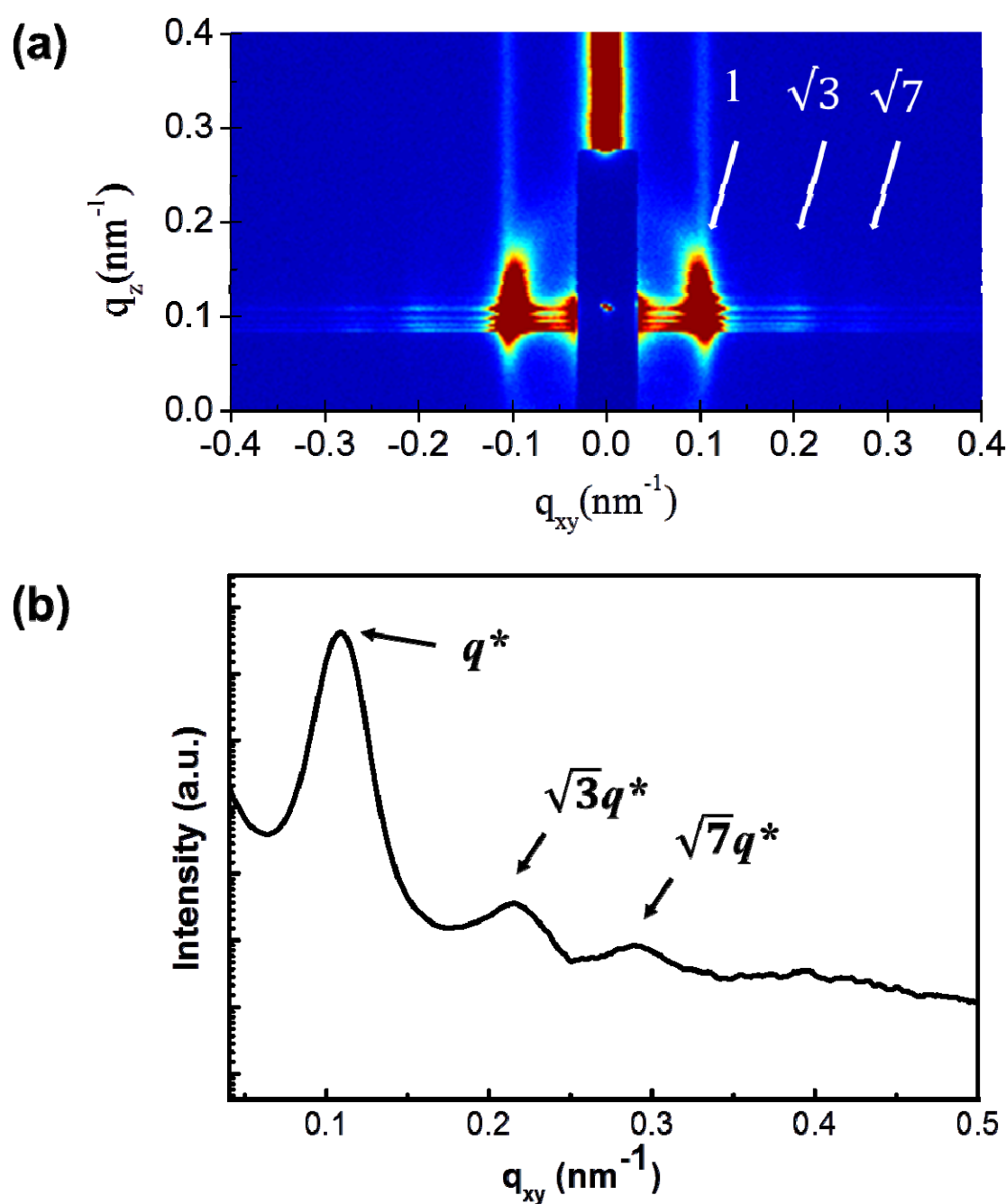


**Fig. S3.** GI-SAXS pattern (a) and one-dimensional GI-SAXS profile along  $q_{xy}$  direction (b) of PS-*b*-P4VP-C film after temperature-programmed solvent vapor annealing as shown in Fig. 4.

Fig. S4 shows the digital camera and optical microscopy (OM) images before and after solvent vapor annealing for PS-*b*-P4VP-C thin film. It is clear that the dewetting of the film did not occur even after a long time solvent vapor annealing (say, 48 h). This indicates that PS-*b*-P4VP thin films employed in this study are stable during the entire solvent vapor annealing process.

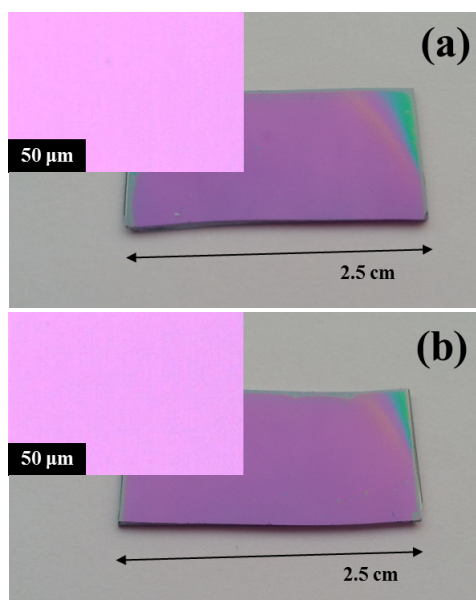


**Fig. S4.** Images of digital camera (a and b) and OM (inset) of PS-*b*-P4VP-C thin film: (a) before and (b) after temperature-programmed solvent vapor annealing as shown in Fig. 4.

### 3. The film thickness depending on the saturated chloroform vapor

A glass vessel of 1000 cm<sup>3</sup> was completely sealed after 5 ml (7.46 g) of chloroform was placed into the vessel at 25 °C. If all of the liquid chloroform were vaporized, the total volume of vaporized chloroform would be 1500 cm<sup>3</sup> ( $= 24450 \text{ cm}^3\text{mol}^{-1} \times 7.46 \text{ g}/119.38 \text{ gmol}^{-1}$ ). However, since the saturated vapor pressure ( $P^*$ ) of chloroform is 196.4 mmHg at 25 °C (see Table S1), the maximum volume of chloroform vapor existing in the chamber should be 181 cm<sup>3</sup> ( $= 1000 \text{ cm}^3 \times 196.4 \text{ mmHg}/760 \text{ mmHg}$ ). This indicates that the amount of liquid chloroform is enough to maintain the saturated vapor pressure inside the closed vessel through the entire experiment.

After the block copolymer film was exposed to the saturated chloroform vapor at 25 °C, the film thickness was increased to 442 nm from 250 nm (see Fig. 4a in the main text). The film thickness change is directly proportional to the sample volume change due to thin film geometry. The sample volume with a thickness of 250 nm and an area (1 cm<sup>2</sup>) before the swelling is  $2.50 \times 10^{-5} \text{ cm}^3$  ( $= 1 \text{ cm} \times 1 \text{ cm} \times 250 \text{ nm}$ ). To make a film thickness of 442 nm, the chloroform vapor volume existing inside the sample should be  $1.92 \times 10^{-5} \text{ cm}^3$ . Since total available chloroform vapor volume inside the vessel at 25 °C is 181 cm<sup>3</sup>, the degree of vapor absorption into the polymer chains is calculated to be  $\sim 10^{-7}$ , which is reasonable for typical solvent absorption into polymer chains.

When the vessel temperature is decreased from 25 to 17 °C,  $P^*$  should decrease from 196.4 to 137.65 mmHg, as shown in Table S1. If the degree of vapor absorption into polymer chains is a little changed with temperature cooling from 25 to 17 °C, the decreased  $P^*$  should result in a decreased volume (and thus, film thickness). From Fig. 4a in the main text, the film decreased from 442 nm to 373 nm with decreasing from 25 to 17 °C. In this case, the decreased volume of the chloroform vapor from 25 to 17 °C is calculated 0.36  $\{ = [(442 - 250) - (373 - 250)]/(442 - 250) \}$ , in which we used the initial thickness of 250 nm before the swelling. This value is similar to that ( $0.3 = (196.4 - 137.65)/196.4$ ) obtained from the decreased  $P^*$  from 25 to 17 °C. A small difference between these two could be explained by the fact that the degree of the absorption of chloroform vapors into the polymer chains at 17 °C is slightly less than that at 25 °C, which is also reasonable.

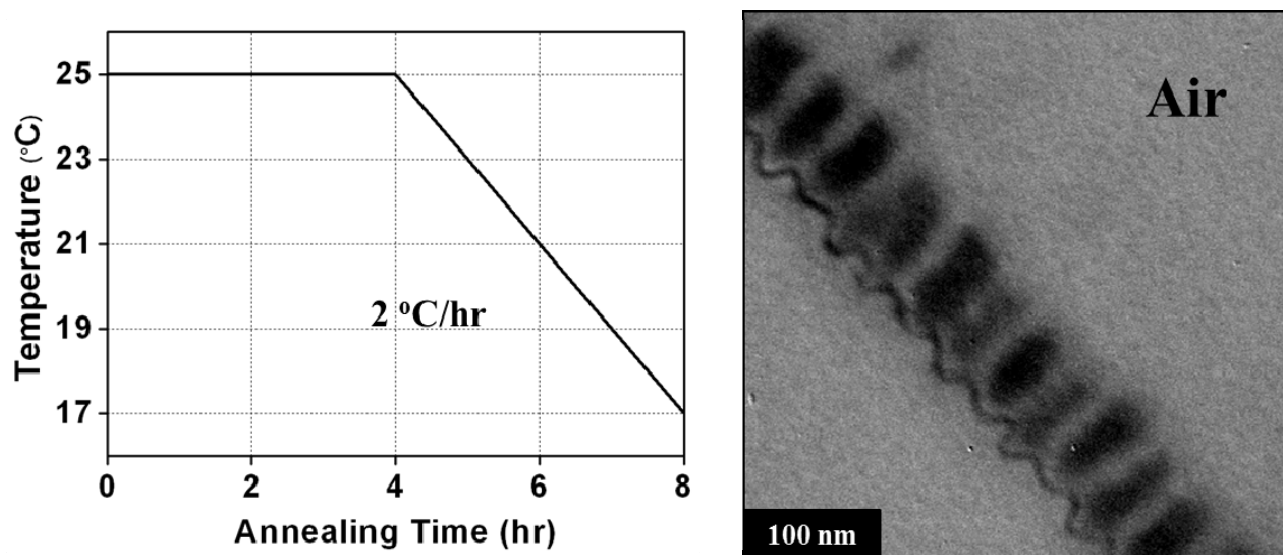
By using the above approach, the decreased film thickness with decreasing temperature as shown in Fig. 4a is explained by the decreased  $P^*$  with decreasing temperature.

**Table S1** Saturated vapor pressures ( $P^*$ ) of chloroform at three different temperatures.

Temperature (°C)	vapor pressure (mmHg) <sup>a)</sup>
25	196.40
21	164.91
17	137.65

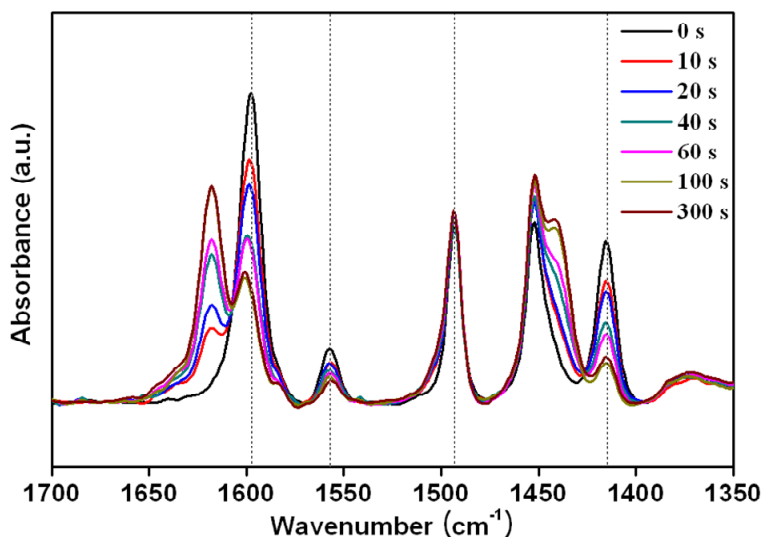
<sup>a)</sup> Calculated from the Antoine equation:  $\log_{10}P^* = A - B / (C + T)$ , where  $A$ ,  $B$ , and  $C$  are Antoine coefficients,  $T$  is the absolute temperature.<sup>3</sup>

Fig. S5 shows cross-sectioned TEM image of thin PS-*b*-P4VP-C film with a thickness of 80 nm after temperature-programmed solvent vapor annealing is performed once. In a relatively thin thickness of film, vertically oriented cylindrical microdomains are obtained when temperature-programmed solvent annealing is done once.



**Fig. S5** Cross-sectional TEM image of PS-*b*-P4VP-C film with a thickness of 80 nm after temperature-programmed solvent vapor annealing.

Fig. S6 Fourier transformed infrared (FTIR) absorption spectra of PS-*b*-P4VP thick films at different immersing times into gold precursor solution ( $\text{HAuCl}_4$ ). The bands at (1596 and 1556  $\text{cm}^{-1}$ ) are from the quadrant stretching of the pyridine rings of P4VP, while those at (1492 and 1413  $\text{cm}^{-1}$ ) are due to the semicircle stretching of the pyridine rings of P4VP.<sup>4-6</sup> The change in the P4VP ring stretching bands clearly manifests the environment change, depending on the binding ratio of the precursor to P4VP. Until the immersing time reaches 100 s, the intensity of the blue shifted bands steadily increases. The coordination of the precursor to the nitrogen in the P4VP chains is saturated after immersing time of 100 s.



**Fig. S6** Fourier transformed infrared (FTIR) absorption spectra of PS-*b*-P4VP-C thick films at different immersing times into HAuCl<sub>4</sub> solutions. All pyridine bands show the blue shifts caused by the coordination of HAuCl<sub>4</sub> and P4VP.

## References

1. S. Sakurai, T. Momii, K. Taie, M. Shibayama, S. Nomura and T. Hashimoto, *Macromolecules*, 1993, **26**, 485-491.
2. F. S. Bates, C. V. Berney and R. E. Cohen, *Macromolecules*, 1983, **16**, 1101-1108.
3. B. E. Poling, J. M. Prausnitz and J. P. O'Connell, *Properties of Gases and Liquids (5th Edition)*, McGraw-Hill: New York, 2001.
4. J. L. Velada, L. C. Cesteros and I. Katime, *Appl. Spectrosc.*, 1996, **50**, 893-899.
5. Y. Ren, T. Murakami, T. Nishioka, K. Nakashima, I. Noda and Y. Ozaki, *Macromolecules*, 1999, **32**, 6307-6318.
6. N. B. Colthup, L. H. Daly and S. E. Wiberley, *Introduction to Infrared and Raman Spectroscopy (3rd edition)*, Academic Press: San Diego, 1990.